Biomaterials 34 (2013) 8589–8598

Contents lists available at ScienceDirect

Biomaterials

journal homepage: www.elsevier.com/locate/biomaterials

Bone formation induced by strontium modified calcium phosphate cement in critical-size metaphyseal fracture defects in ovariectomized rats

Ulrich Thormann [a,b,1], Seemun Ray [a,1], Ursula Sommer [a], Thaqif ElKhassawna [a], Tanja Rehling [a], Marvin Hundgeburth [a], Anja Henß [c], Marcus Rohnke [c], Jürgen Janek [c], Katrin S. Lips [a], Christian Heiss [a,b], Gudrun Schlewitz [a,b], Gabor Szalay [a,b], Matthias Schumacher [d], Michael Gelinsky [d], Reinhard Schnettler [a,b], Volker Alt [a,b,*]

[a] Laboratory of Experimental Trauma Surgery, Justus-Liebig-University, Giessen, Germany
[b] Department of Trauma Surgery, University Hospital Giessen-Marburg GmbH, Campus Giessen, Germany
[c] Institute for Physical Chemistry, Justus-Liebig-University Giessen, Giessen, Germany
[d] Centre for Translational Bone, Joint and Soft Tissue Research, Medical Faculty and University Hospital, Technische Universität Dresden, Dresden, Germany

ARTICLE INFO

Article history:
Received 11 June 2013
Accepted 9 July 2013
Available online 29 July 2013

Keywords:
Biomaterial
Strontium
Calcium phosphate
Bone
Fracture

ABSTRACT

The first objective was to investigate new bone formation in a critical-size metaphyseal defect in the femur of ovariectomized rats filled with a strontium modified calcium phosphate cement (SrCPC) compared to calcium phosphate cement (CPC) and empty defects. Second, detection of strontium release from the materials as well as calcium and collagen mass distribution in the fracture defect should be targeted by time of flight secondary ion mass spectrometry (TOF-SIMS). 45 female Sprague–Dawley rats were randomly assigned to three different treatment groups: (1) SrCPC ($n = 15$), (2) CPC ($n = 15$), and (3) empty defect ($n = 15$). Bilateral ovariectomy was performed and three months after multi-deficient diet, the left femur of all animals underwent a 4 mm wedge-shaped metaphyseal osteotomy that was internally fixed with a T-shaped plate. The defect was then either filled with SrCPC or CPC or was left empty. After 6 weeks, histomorphometric analysis showed a statistically significant increase in bone formation of SrCPC compared to CPC ($p = 0.005$) and the empty defect ($p = 0.002$) in the former fracture defect zone. Furthermore, there was a statistically significant higher bone formation at the tissue–implant interface in the SrCPC group compared to the CPC group ($p < 0.0001$). These data were confirmed by immunohistochemistry revealing an increase in bone-morphogenic protein 2, osteocalcin and osteoprotegerin expression and a statistically significant higher gene expression of alkaline phosphatase, collagen10a1 and osteocalcin in the SrCPC group compared to CPC. TOF-SIMS analysis showed a high release of Sr from the SrCPC into the interface region in this area compared to CPC suggesting that improved bone formation is attributable to the released Sr from the SrCPC.

1. Introduction

The treatment of osteoporotic fractures and particularly of osteoporotic fractures with bone defects remains a critical challenge. Biomaterials with the potential to stimulate bone healing have gained interest to improve healing and the treatment outcome for patients with osteoporotic fractures [1]. Injectable calcium phosphate cements have been used in bone surgery since many years based on their osteoconductive properties to stimulate new bone formation [2]. Strontium (II) (Sr^{2+}) has been shown to effectively both stimulate bone formation and inhibit osteoclastic activity and has been introduced into all day clinical practice as oral strontium ranelate medication against osteoporosis [3,4]. Local administration of strontium mainly from functionalized titanium implant surfaces [5–10] or from strontium-substituted hydroxyapatite coatings [11,12] gained interest due to the positive effects of strontium on new bone formation for better implant fixation.

* Corresponding author. Department of Orthopaedic Trauma Surgery, Justus-Liebig-University Giessen, Rudolf-Buchheim-Str. 7, 35385 Giessen, Germany. Tel.: +49 (0) 641 985 44 601; fax: +49 (0) 641 985 44 609.
E-mail address: volker.alt@chiru.med.uni-giessen.de (V. Alt).
[1] Shared first co-authorship as both authors contributed equally to this work.

0142-9612
http://dx.doi.org/10.1016/j.biomaterials.2013.07.036

We recently showed the possibility to generate a strontium (II) modified calcium α-tricalcium phosphate based phosphate cement (SrCPC) in which the $CaCO_3$ portion in the precursor mixture is replaced completely with strontium carbonate ($SrCO_3$, 99.994%), resulting in Sr/Ca ratio of 0.123 [13]. The intention of this recently developed composite material is to use the osteoconductive calcium phosphate cement as a drug carrier for the local release of strontium into bone defects in order to leverage the osteoanabolic and anti-osteoclastic activity not in a systemic but local environment to achieve high strontium concentrations with subsequent enhancement of new bone formation.

In vivo evaluation of SrCPC effects on new bone formation in osteoporotic bone requires a clinically relevant animal model that mimics osteoporotic fractures. Recently, we published a rat model with a critical size defect in the distal metaphyseal femur in which biomaterials can be tested [14]. This model shows important reduction in bone mineral density (BMD) of both spine and femur after bilateral ovariectomy and special diet deficient in calcium, phosphorus and vitamin D3-, soy- and phytoestrogen-free compared to sham animals. The osteotomy addresses the metaphyseal region of the distal femur respecting the fact that mainly metaphyseal regions are affected by osteoporotic fractures and uses the clinically relevant surgical technique of plate fixation of such a fracture defect.

Time of flight secondary ion mass spectrometry (TOF-SIMS) originates from materials science with increasing applications in life science due to its ability to assess chemical composition of solid surfaces down to about 100 nm lateral resolution [15,16]. In brief, a high energetic cluster ion beam is scanning over the sample surface in order to release molecules, atoms and ions that subsequently fly away from the sample surface due to the ion impact. The ions can then be collected by an electrical field and are analyzed in a time of flight analyzer by their mass to charge ratio which enables to visualize strontium and calcium distribution in bone.

The first intention of this study was to evaluate the effects on new bone formation of strontium modified calcium phosphate cement (SrCPC) compared to a strontium free calcium phosphate cement of otherwise similar composition (CPC) and an empty defect control group with the use of the above mentioned clinically relevant rat model [14]. The second intention was to use TOF-SIMS technology to detect strontium release from the materials as well as calcium and collagen mass distribution in the defect area.

2. Materials and methods

2.1. Study design and general information

All interventions were performed in full compliance with the institutional and German protection laws and approved by the local animal welfare committee (Reference number: V 54 – 19 c 20-15 (1) GI 20/28 Nr. 108/2011). 45 female Sprague–Dawley rats were randomly assigned to three different treatment groups: (1) strontium modified calcium phosphate (SrCPC) ($n = 15$), (2) calcium phosphate cement (CPC) ($n = 15$), and (3) empty defect control ($n = 15$). The animals underwent induction of osteopenic bone status by bilateral ovariectomy combined with a multi-deficient diet as previously described [14,17,18]. Three months after ovariectomy and multi-deficient diet, a 4 mm defect in the distal femur metaphysis was created that was stabilized with a mini-plate. The defect was subsequently filled either with SrCPC, CPC or left empty (Fig. 1). The femurs were harvested after 6 weeks and histomorphometrical assessment including immunohistochemistry, enzyme histochemistry, molecular-biological analysis and TOF-SIMS analysis for detection of strontium, calcium and collagen was performed.

2.2. Calcium phosphate cement (CPC) and strontium (II)-modified calcium phosphate cement (SrCPC)

Calcium phosphate cement (CPC) as well as a strontium (II)-modified cement (SrCPC) were used in this study. Synthesis and material properties have been described recently in detail elsewhere [13]. In brief, CPC precursor was composed of α-tricalcium phosphate (α-TCP; α-$Ca_3(PO_4)_2$), calcium hydrogenphosphate ($CaHPO_4$), calcium carbonate ($CaCO_3$) and hydroxyapatite ($Ca_{10}(PO_4)_6(OH)_2$) as first described by Driessens and co-workers [19]. In case of strontium-containing SrCPC, $CaCO_3$ was replaced completely with strontium carbonate ($SrCO_3$, 99.994%, Alfa Aesar, Karlsruhe, Germany), resulting in the formation of a Sr^{2+}-substituted apatite cement matrix with a Sr/Ca ratio of 0.123. Cement precursor powders were supplied by InnoTERE GmbH (Radebeul, Germany) and were sterilized by γ-radiation at 25 kGy. Prior to implantation, cement powder was manually mixed with 4 wt.% aqueous Na_2HPO_4 solution using a liquid-to-powder-ratio of 0.40 and 0.35 ml/g for CPC and SrCPC, respectively.

2.3. Animals and surgical procedure

10 weeks old healthy female Sprague–Dawley rats were purchased from Charles River (Sulzfeld, Germany), with an initial weight of 250–290 g. All animals were randomly assigned to the three treatment groups. Animals underwent an acclimatization period of four weeks before induction of osteopenic bone status as described previously [17,18]. Briefly, rats were ovariectomized bilaterally with a dorsal approach. Thereafter, the animals received a low calcium-, phosphorus- and vitamin D3-, and soy- and phytoestrogen-free multi-deficient diet (Altromin-C1034, Altromin Spezialfutter GmbH, Lage, Germany), for 12 weeks.

A wedge-shaped osteotomy was performed on the distal end of the left femur as previously described [14]. In brief, the distal femur was fixed laterally with 7-hole T-shaped mini-plate (Leibinger® XS-mini-plate, Stryker, Schökirchen, Germany). Then the osteotomy at the distal metaphyseal area with creation of a wedge-shaped defect with a lateral length of 4 mm and a medial gap of 0.35 mm using an ultrasound bone saw (Piezosurgery® 3, Saw blade OT7S-3, Mectron, Köln, Germany) was performed. The defect was then treated according to the study protocol and the animals either received SrCPC, CPC or no biomaterial (Fig. 1). Postoperatively, animals continued receiving the deficient diet until euthanized at 6 weeks post femur surgery. Animals were euthanized under inhalation of CO_2 after general anesthesia.

2.4. End-point and specimen preparation

Animals were euthanized 6 weeks post femur surgery. The left femora were then harvested, and all surrounding soft-tissue was removed. Only samples with intact fixation plates were used for further analysis.

2.5. TOF-SIMS

Measurements were done with a TOF-SIMS 5–100 machine (IONTOF, Münster, Germany) on Technovit section (see chapter "Histological analysis"). The machine is equipped with a 25 keV Bi-cluster ion gun for surface analysis. The maximum dimension for the primary ion raster mode is 500 × 500 μm². For survey images, so called stage scans, were used. Single ion images of 300 × 300 μm² were merged to a big mass image of 7.0 × 14.5 mm² for the empty defect, 6.7 × 14.2 mm² for CPC and 8.1 × 13.6 mm² for the SrCPC group. With a pixel density of 100/mm, the primary ion gun runs in the high current bunched (hc-bu) mode with highest mass resolution and a lateral resolution of about 10 μm for this large survey images. For more detailed images, the low current bunched (lc-bu) mode with a lateral resolution of 2 μm was used. The pixel density was 1000/mm and single frames of 300 × 300 μm² were assembled to survey images of 1.8 × 0.9 mm². As primary ion species Bi^{3+} was used. Data evaluation was done with the Surface Lab 6.3 software (IONTOF, Münster, Germany) delivering detailed mass maps of the analyzed surface. In one mass image usually only the distribution of one selected mass is shown. Within this image, bright and dark pixels represent a high and low count rate of this mass, respectively. For more detailed information about this method the reader is referred to the literature [16].

Mass distribution analysis of Sr^+, Ca^+, and of $C_4H_8N^+$ which was shown to correlate with collagen I [20] was performed. Furthermore, an overlay image of the collagen and Ca signal was depicted.

2.6. Histological analysis and histomorphometry

For histological analysis, the harvested femurs were fixed in phosphate- buffered 4% paraformaldehyde and stored at 4 °C until processing. Samples were then embedded in Technovit® 9100 NEU according to the manufacturers protocol (Heraeus Kulzer, Hanau, Germany). After embedding, Technovit blocks were sectioned into 5 μm thick slices with the aid of Kawamoto's film (Section-Lab Co. Ltd., Japan) to keep the biomaterials intact. For histological and histomorphometrical analysis these sections were stained with movat-pentachrome as described earlier [21].

Two regions of interest (ROIs) were used for histomorphometric evaluations (Fig. 2). The first ROI was made by directly tracing over the material followed by a 100 pixels increase to include the biomaterial–tissue interface. The second ROI comprised the entire initial wedge-shaped osteotomized defect area to assess the new bone formation within the former fracture defect area. With the help of Adobe Photoshop CS6, the measurements for area of bone, ROIs, implant, and the void were made respectively to determine bone versus tissue ratio (BV/TV). A count for tartrate-resistant acid phosphatase (TRAP) positive cells was also performed. The consecutive sections were then used for all described methods. The measurements were done blind folded with regards to the test groups.

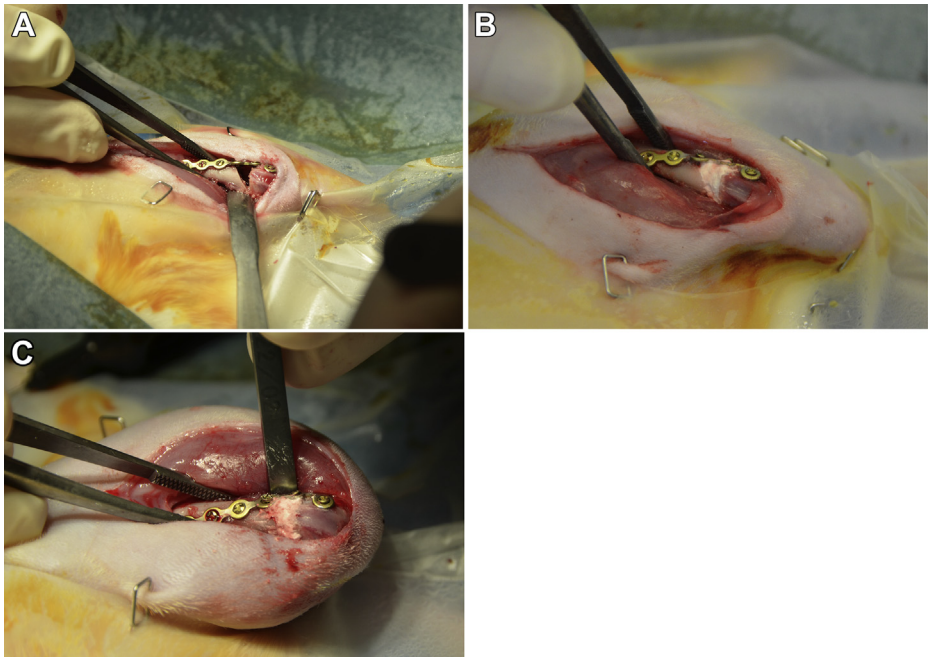

Fig. 1. Intraoperative appearance of the distal femur of the empty defect (A), defect filled with SrCPC (B) or CPC (C) stabilized with a T-shape mini-plate.

2.7. Immunohistochemistry

Immunohistochemistry was carried out with the following antibodies: Rabbit Anti-BMP2 Polyclonal Antibody (AP20597PU-N; Acris, Herford, Germany), Rabbit Anti-Osteoprotegerin Polyclonal Antibody (250800; Abbiotec, San Diego, CA, USA), Rabbit Anti CD254/RANKL Polyclonal Antibody (AP30826PU-N; Acris, Herford, Germany), Rabbit Anti CD31 Antibody (250590; Abbiotec, San Diego, CA, USA).

Goat Anti-Rabbit (BA-1000, Vector) was used as a secondary antibody followed by a Vectastain ABC kit (Elite PK-6100, Standard, Vector Laboratories, Burlingame, CA, USA). Finally visualization was done using Nova Red (SK4800, Vector Laboratories,

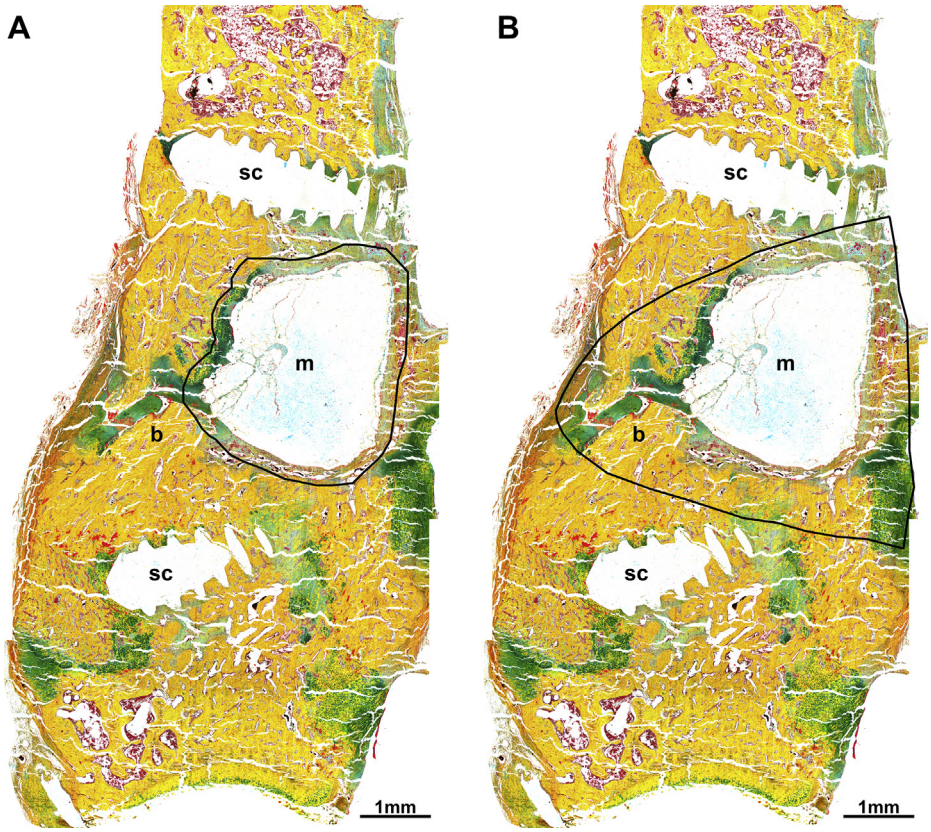

Fig. 2. Schematic diagram of a movat-pentachrome staining of undecalcified technovit sections with the two regions of interest (ROIs) for quantitative histomorphometric evaluation: First ROI (within black outline) was used to evaluate the new bone formation at the tissue-implant interface (A). The second ROI (enclosed within black outline) comprises the entire defect region to examine the new bone formation in the initial fracture defect (B). Specific regions are labeled as follows: b, bone; m, material; sc, screw.

Burlingame, CA, USA) and hematoxylin (Shandon Inc., Pittburgh, USA) was used as a counterstain.

2.8. Enzymehistochemical analysis

TRAP staining was used to investigate the osteoclast activity. After deplastification, the samples were treated with sodium acetate buffer and incubated in Napthol-AS-TR phosphate (N6125-1G, Sigma, Germany) in N–N-Dimethyl formamide (Sigma Aldrich) and sodium tartrate (Merck, Germany) with Fast Red TR salt (Sigma Aldrich) at 37 °C for 1 h. This was followed by counterstaining with hematoxylin (Shandon Inc., Pittsburgh). TRAP-positive cells were analyzed in both the ROI's.

Images were taken using Axioplan 2 Imaging system (Carl Zeiss, Germany) with a Leica DC500 camera (Leica, Bensheim, Germany), acquired with Leica IM1000 software and processed using Adobe photoshop CS6.

2.9. mRNA preparation and gene analysis

Left femora obtained 6 weeks after operation were snap frozen in RNA*later*® RNA Stabilization Solution (Ambion, CA, USA) and stored at −80 °C until RNA isolation for expression analysis of the following target genes for new bone formation:

1. Alkaline phosphatase (ALP) as an osteoblast marker indicating mineralization of bone; 2. Osteocalcin (OCN) as a noncollagenous protein secreted by osteoblasts which plays a role in mineralization and calcium ion homeostasis; 3. Collagen type 10 alpha1 (Col10a1) as a hypertrophic chondrocytes marker; 4. Runt-related transcription factor 2 (Runx2) as essential protein for osteoblastic differentiation; 5. Collagen type I alpha1 as major component of type I collagen, (Col1a1).

The following target genes were analyzed for osteoclast processes: 1. TNFSF11 gene (RANKL, RANK ligand as a member of the tumor necrosis factor (TNF) cytokine family, which is a ligand for osteoprotegerin and functions as a key factor for osteoclast differentiation and activation) 2. TNFRSF11B gene (osteoprotegerin; OPG; as decoy receptor for RANKL and thereby neutralizing its function in osteoclastogenesis) 3. carbonic anhydrase as an osteoclasts marker involved in bone matrix dissolution.

β2-microglobulin (B2M) was used as a reference gene. Primer sequences are provided in the Supplemental Table 1.

RNA isolation was done from the entire defect region from each sample using Lipid Tissue Mini Kit® (Qiagen, Hilden, Germany) according to the manufacturer's protocol. RNA quality and quantity was measured using Nanodrop2000® (Thermo scientific, Schwerte, Germany) and Qubit 2.0 fluorometer® (Invitrogen, Darmstadt, Germany). 0.5 μg of RNA was reverse-transcribed to cDNA with the Quantitect® Kit (Qiagen, Hilden, Germany) as described in the manufacturer's protocol. Primers were designed to amplify 72–191 bp long amplicons within the coding sequences of the above described target genes.

Quantitative polymerase chain reaction (qPCR) analysis was performed using the LightCycler detection system (Roche, Mannheim, Germany) in combination with the Quantifast SYBR Green PCR Mastermix® (Qiagen, Hilden, Germany) for Runx2-, ALPL-, OCN-, Col1a1-, Col10a1-, RANKL- and OPG-primers and B2M reference gene-primers. Roche LightCycler Kit® was used for Car2-primers and B2M- reference gene-primers. For RT-PCR, 1 μl cDNA, 5 μl Quantifast SYBR Green PCR Mastermix or 2 μl Roche 5× PCR Mastermix and 0.1 μl of each primer (20 μM) were supplemented with RNase free H_2O to a final volume of 10 μl.

The thermal cycling program with Quantifast Mastermix® comprised one initial denaturation step of 5 min at 95 °C, followed by 40 cycles of 10 s at 95 °C and 30 s at 60 °C. Finally, a melting curve was performed to verify the product's specificity and identity.

qPCR analysis using Roche PCR Mastermix® implemented an initial denaturation step of 10 min at 95 °C followed by a cycling protocol which included a denaturation step at 95 °C for 5 s and an annealing step at 60 °C for 5 s followed by a final extension at 72 °C for 5 s carried out for 40 cycles. A melting curve analysis was done to determine the product specificity. All analyses were done in duplicate and the means were used for further calculations. The following controls were performed: every sample processed without reverse transcription (−RT) to control for contamination with genomic DNA and RT-PCR runs without template (H_2O). Specificity of amplification was confirmed by melting curve analyses and 2% agarose gel electrophoresis.

The amplification efficiency for the tested primer pairs varied from 1.93 to 2.00 which are the expected values for compared genes. The relative gene expression ratio for each gene was calculated using the REST© method based on the PCR efficiency (E) and Ct of a sample compared with the control, and expressed in comparison to the reference gene, according to Pfaffl's mathematical model: Ratio = (E_{target}) ΔCt target (control-sample)/(E_{ref}) ΔCt ref (control-sample) [22].

2.10. Statistical analysis

Histomorphometric results are presented as mean ± standard error of the mean (SEM) with minimum and maximum values [mean ± SEM; min.: maximum] and analyzed using the Statistical Package PASW 21.0 (SPSS Inc., USA). Data were not found normally distributed and Mann–Whitney U unpaired nonparametric data with bonferroni correction. Expression analysis is presented as box plots and were analyzed using REST© method. *P*-values of less than 0.05 were chosen to indicate significance.

3. Results

3.1. Clinical observations

39 of the 45 animals survived the entire observation period which represented 11 animals of the control, 15 animals of the SrCPC and 13 animals of the CPC group. In these animals clinical healing of the surgical wounds and recovery of mobility of the animals progressed uneventfully with no visible adverse effects in all groups until the end of the observation period of 6 weeks post femur surgery. Three animals were lost during anesthesia, one animal died directly after ovariectomy and two other rats after femur surgery.

At the time of femur harvesting, plate breakage was noted in 2 of the remaining 11 animals in the control group, in 4 of 15 animals of the SrCPC and in 7 of 13 animals in the CPC group without any statistically significant differences between the groups (empty defect vs. CPC: $p = 0.58$; empty defect vs. SrCPC: $p = 0.61$; SrCPC vs. CPC: $p = 0.06$).

3.2. TOF-SIMS analysis

Visualization of strontium distribution by TOF-SIMS was possible in all three groups (Fig. 3). The evaluation of the strontium distribution of the empty defect shows that there is a natural Sr background count rate of about 11 counts while CPC implants were found to exhibit a mean Sr count rate of 24 counts. The highest Sr count rate of about 3000 counts was obtained in the center region of the Sr^{2+} modified SrCPC implant. There were count rates of about 80 counts in the biomaterial–tissue interface in a distance up to 1 mm to the biomaterial with a Sr concentration gradient to all sides of the implant. The Sr content decreased with increasing distance from the implant. In a distance of up to 6 mm to the implant, an increased Sr concentration could still be detected.

Ca could be found in cortical bone in all three groups and in the CPC and SrCPC material itself. In all specimens bone marrow areas were almost free of Ca signals. Within the region of newly formed bone in the interface region, Sr and Ca were in the same area as the collagen signal.

3.3. Histomorphometry

Histomorphometric analysis showed a statistically significant increase in the bone formation for the CPC [0.042 ± 0.03; 0.01:0.09] ($p = 0.01$) and the SrCPC [0.11 ± 0.01; 0.1:0.15] ($p = 0.002$) treatment group compared to the empty defect [0.004 ± 0.002; 0.0:0.01] in the former fracture defect zone (Fig. 4A). SrCPC treated animals showed a statistically higher new bone formation in relation to the defect areas filled with CPC ($0 = 0.005$).

Furthermore, there was more bone formation at the bone-biomaterial interface region for the SrCPC [47.5 ± 13.8; 29.5:64.5] compared to CPC [6.4 ± 1.5; 4.9:8.2] which was also statistically significant ($p < 0.0001$) (Fig. 4B).

TRAP-positive cells were also found to be significantly higher in the SrCPC group [87.5 ± 21.9; 43:100] in comparison to the CPC group [CPC: 43.7 ± 2.6; 40:46] ($p = 0.033$) and the empty defect control group [30.6 ± 2.5; 26:33] ($p = 0.005$) (Fig. 5). Most of the TRAP-positive cells were found in at the biomaterial–tissue interface region.

3.4. Histology

The animals of the SrCPC and the CPC group showed the implanted biomaterial in the correct position where the wedge-shaped defects were created initially at the distal metaphyseal

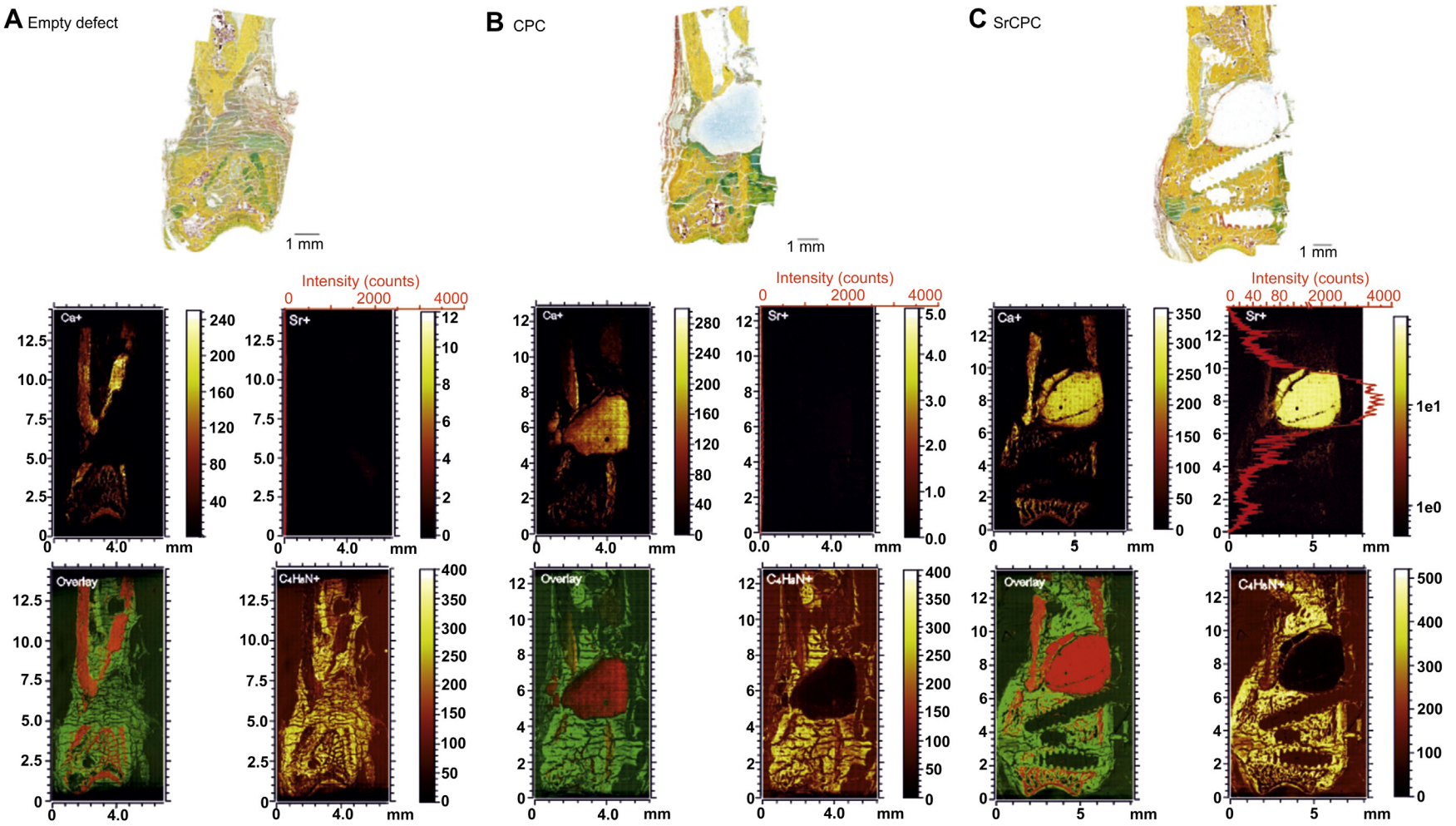

Fig. 3. Overview of movat-pentachrome stained sections of representative specimens of the empty defect (A), CPC (B) and SrCPC group (C) used for TOF-SIMS analysis. The small images under the overview images show mass distribution of Ca^+ (upper left), Sr^+ (upper right), C4H8N$^+$ (lower right) and an overlay image of the Ca^+ and of the $C_4H_8N^+$ signal (lower left). For better distribution analysis of Sr^+, the local count rates of Sr^+ are plotted versus the *y*-axis and placed over the Sr-images.

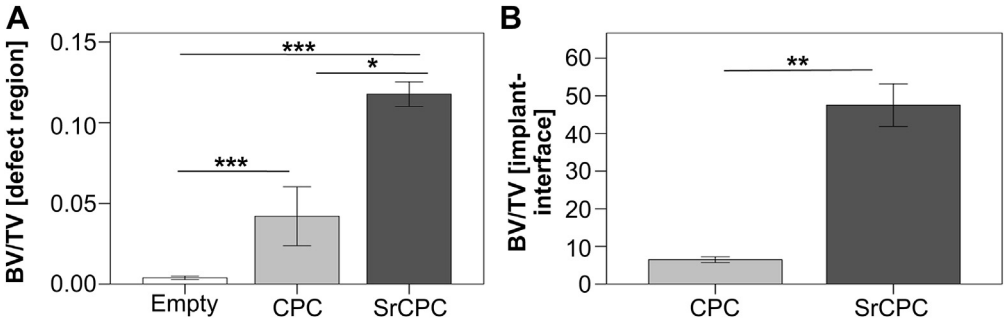

Fig. 4. Histomorphometrical analysis of new bone formation of SrCPC, CPC and empty control group in the initial fracture defect zone (A) and at the tissue–biomaterial interface (B). Asterisks indicate (*) $p < 0.05$, (**) $p < 0.01$ and (***) $p < 0.001$, respectively.

femur region (Fig. 6 B,C). Fragmentation of the material was seen in 5 of 7 animals in the SrCPC group. In all these animals, the fragmented biomaterial was surrounded by osteoid, cartilage and fibrous tissue at the interface region. In the CPC group only 2 out of 7 animals showed fragmentation of the material of which one had only very little fragmentation and was surrounded mostly by fibrous tissue.

Unmineralized osteoid was the most common tissue type found in the defect region in the SrCPC group, mainly in vicinity of the biomaterial and on the medial aspect of the distal femur. The CPC group showed comparatively less osteoid formation and the empty group almost lacked of osteoid in the initial defect area. Furthermore, mainly bone and cartilage tissue with hypertrophic chondrocytes were found in the SrCPC group in the defect region surrounding the biomaterial (Fig. 6E). In the animals of the CPC group mainly cell dense fibrous tissue and proliferating chondrocytes were the predominant types (Fig. 6D). There was noticeably less cartilage formation in the empty defect control group compared to the other two groups. In context to the medial side of the osteotomy (apex of the wedge-shaped defect), the gap was filled with cartilage and connective tissue in the SrCPC group whereas in the CPC group, and to a greater extent in the control group, large shifting of the cortical bones were seen. This space was predominantly occupied with fibrous tissue.

3.5. Immunohistochemical analysis

Immunohistochemical staining revealed a strong positive BMP2 expression in the SrCPC group mainly in direct vicinity of the biomaterial towards the biomaterial-metaphyseal cancelous (distal) bone and mid cortical regions. An almost negligible expression was seen in CPC and in the control group (Fig. 7)A–C. An increased expression of OPG and OCN was also seen at the distal and mid cortical region of the fracture gap in the SrCPC group compared to the two other groups (Fig. 7)D–I. Furthermore, a simultaneous reduction in the RANKL expression was detected in the SrCPC group.

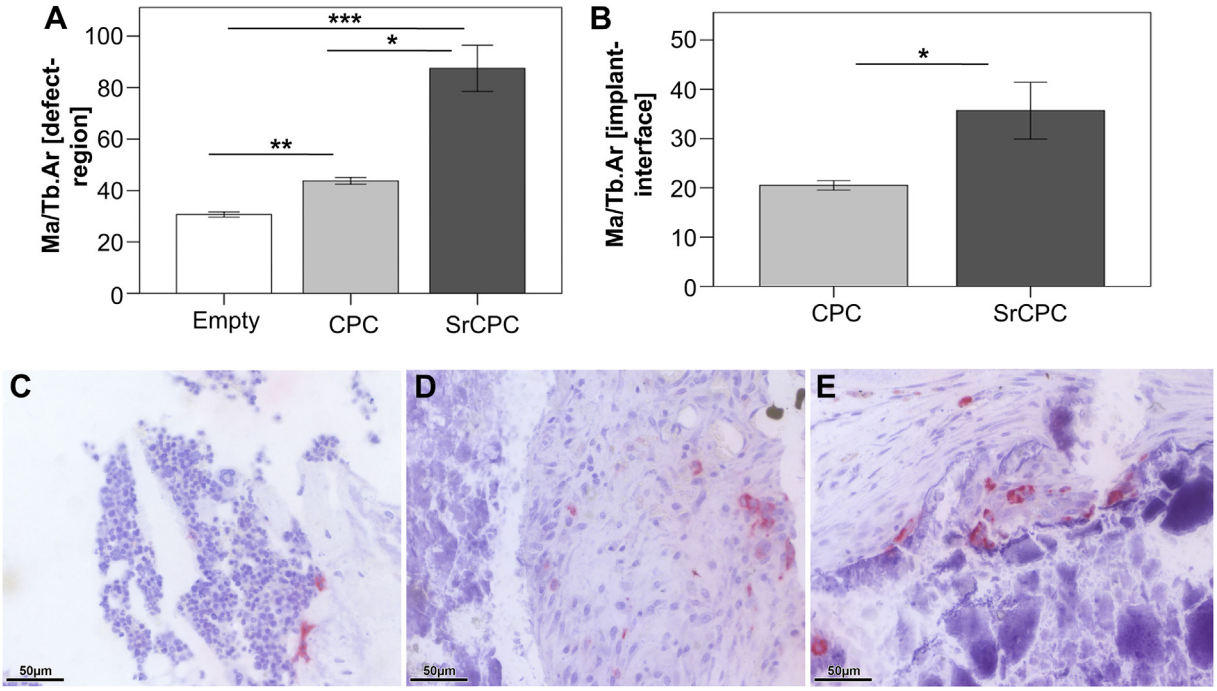

Fig. 5. Macrophage count based on tartarate resistance acid phosphatase (TRAP) staining over trabecular area (Ma/Tb.Ar) of SrCPC, CPC and empty control groups in the initial fracture defect zone (A) and at the tissue–biomaterial interface (B). The asterisks indicate (*) $p < 0.05$, (**) $p < 0.01$ and (***) $p < 0.001$ respectively. Photomicrographs of histologically stained sections with TRAP showing an elevated distribution of red stained cells in SrCPC group (E) when compared to CPC (D) and (E) empty control group (For interpretation of the references to color in this figure legend, the reader is referred to the web version of this article.).

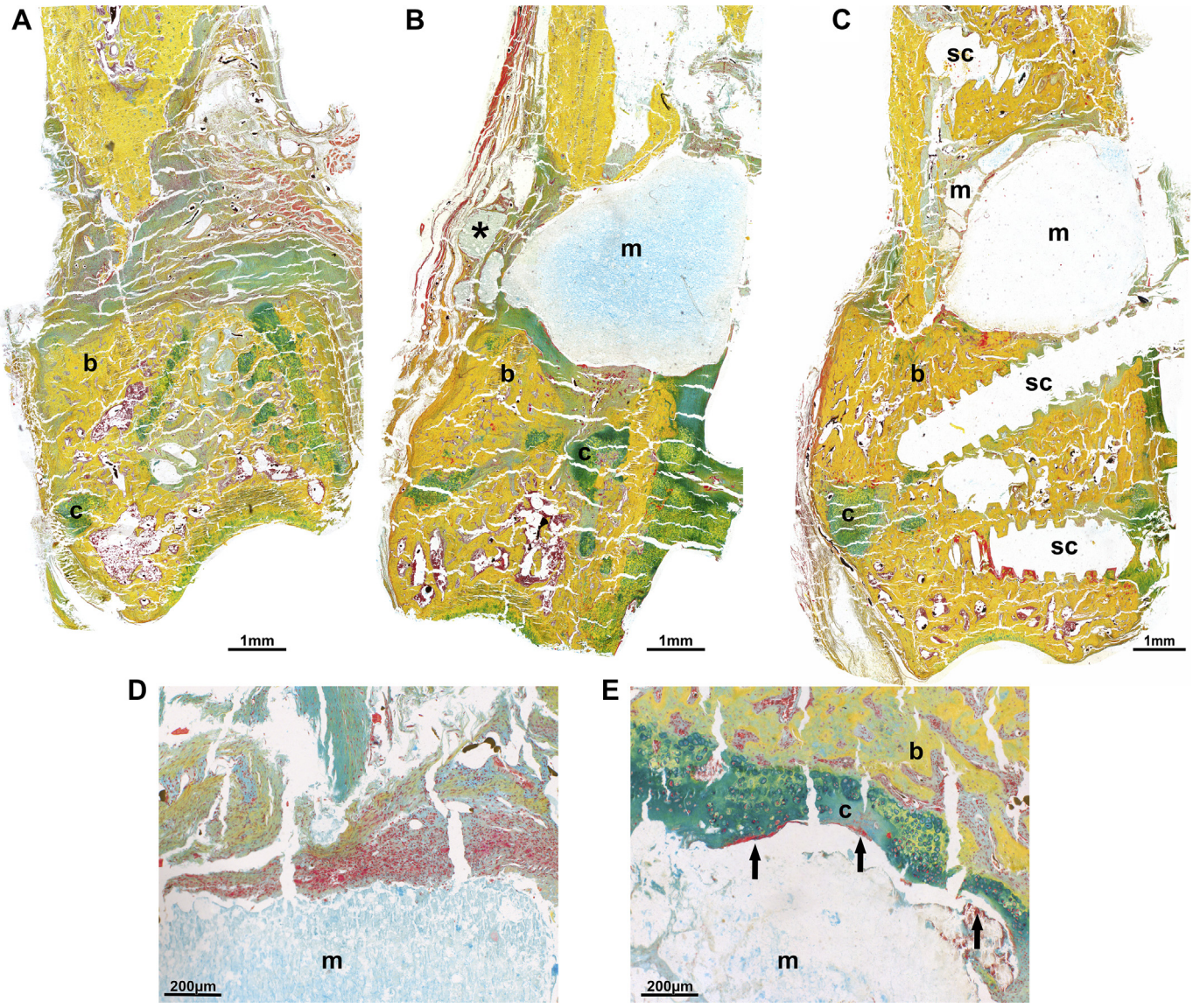

Fig. 6. Movat-pentachrome photomicrographs showing overview of histological sections of empty defect (A), CPC (B) and SrCPC (C). Enlarged images at the biomaterial interface depicting large amounts of fibrous connective tissue and proliferating chondrocytes in the CPC group (D) in contrast to new bone formation with large amounts of cartilage and osteoid in the SrCPC group (E). The hypertrophic chondrocytes were the most abundant. Specific regions are labeled as follows: b, bone; c, cartilage; m, material; sc, screw; * indicates material in the soft-tissue; arrow indicating the osteoid formation.

The analysis of new blood vessel formation using CD31 antibody revealed a comparatively higher number of positively stained vessels in the SrCPC group in comparison to the CPC group. An increased positive reaction was seen with an increase in the biomaterial fragmentation (SrCPC) thereby leading to an increase in the granulation tissue and thus leading to an increased vessel formation. Based on this principle, the empty defect which was filled predominantly with the granulation tissue, showed a comparatively higher CD31 expression (Fig. 7J–L).

3.6. Molecular biology

The expression of several genes was determined by qPCR. Results showed expression differences between the CPC and SrCPC groups normalized to B2M gene expression (Fig. 8). Expression of ALP as an osteoblast marker indicating mineralization of bone was higher in the SrCPC group when compared to the CPC group ($p = 0.027$). Osteocalcin expression analysis indicates a higher osteocalcin expression in the SrCPC group when compared to the CPC group ($p \leq 0.001$). Expression of Col X in SrCPC was significantly higher than that of the CPC ($p = 0.03$) (Fig. 8A). Runx2 and Col1a1 expression analysis showed no significant difference between the SrCPC and the CPC group.

RANKL expression analysis revealed no significant difference between the two experimental groups. Expression levels of OPG were not significantly different between the groups. Moreover, carbonic anhydrase is an osteoclast marker involved in bone matrix dissolution, was not found to be significantly expressed either (Fig. 8B).

4. Discussion

The intention of this study was to investigate the *in vivo* effects of a strontium modified calcium phosphate cement in a critical size defect in the metaphyseal area of the distal femur in ovariectomized rats. Both CPC and SrCPC revealed a statistically significantly enhanced new bone formation compared to the empty defect in the defect region. It could be shown that the SrCPC treated animals

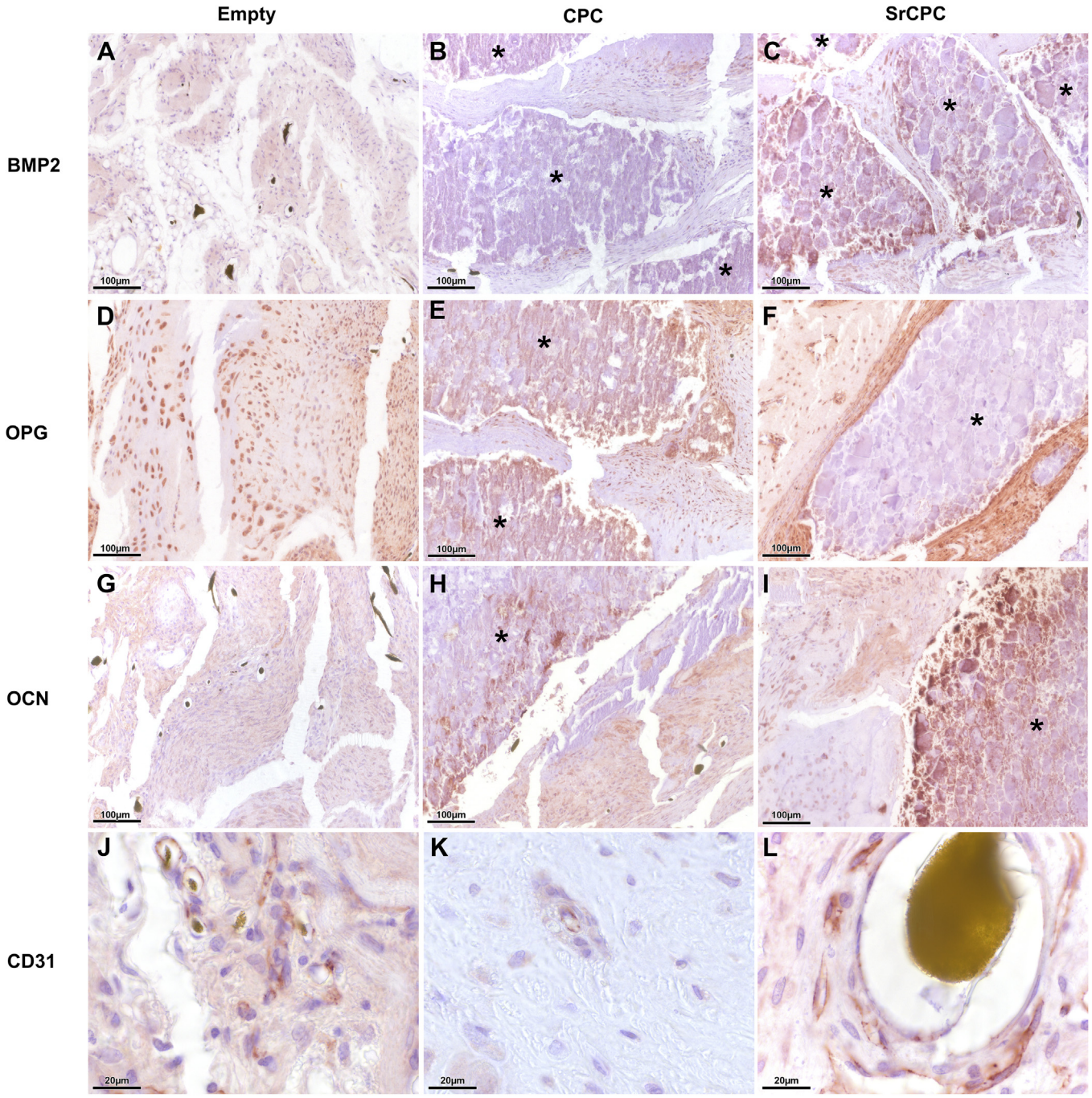

Fig. 7. Immunohistochemistry on undecalcified technovit sections showing an increased expression of biomarkers involved in bone formation in SrCPC group. Increased expression of BMP2 (C); OPG (F); osteocalcin (I); CD31 (L) was seen at the tissue implant interface in the SrCPC group in comparison to the CPC (B, E, H, K) and empty control group (A, D, G, J). * indicates the biomaterial in the defect region of SrCPC and CPC group.

exhibited a statistically significant higher new bone formation both at the biomaterial–bone interface and in the entire fracture defect area compared to CPC suggesting that the local release of Sr from SrCPC is able to positively influence osteogenesis. Immunohistological and molecular-biological investigations could confirm the enhanced new bone formation activities in the SrCPC group with enhanced expression of BMP2, osteocalcin and OPG compared to CPC and the empty defect control group. High CD31 expression suggests concomitant new blood vessel formation in the SrCPC group.

These finding are in line with better new bone formation and implant-bone contact of other *in vivo* studies on strontium-substituted hydroxyapatite coatings [11] or strontium-doped hydroxyapatite bone graft extender [23]. Recently, Andersen et al. showed that the local delivery of strontium from surface functionalized titanium implants could enhance bone-to-implant contact for implants in the femoral shaft of healthy female Wistar rats [5]. The authors concluded that strontium can be released into the local milieu of osseointegrating implants to accelerate bone ingrowth into the implant surface. However, all previous works did not analyze the *in vivo* release of Sr into the bone which could be done in our study with the help of TOF-SIMS. By this means, the high Sr concentration in the interface region of the SrCPC implant

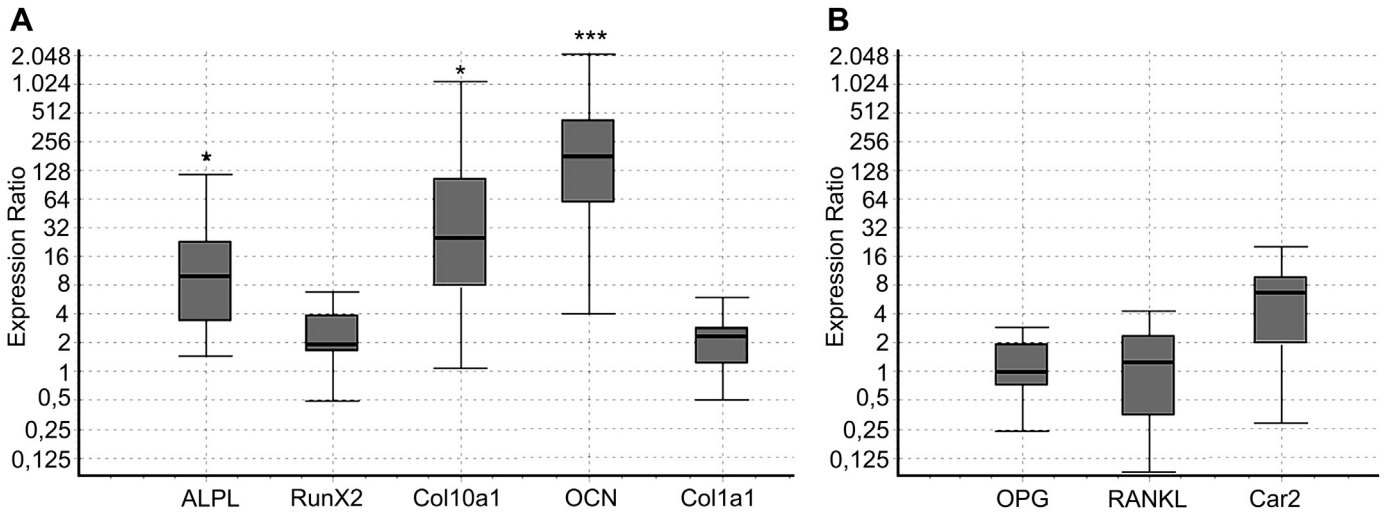

Fig. 8. Relative gene expression analysis between SrCPC and CPC. Alkaline phosphatase (ALP), Runt-related transcription factor 2 (Runx2), collagen type X alpha1 (Col10a1), osteocalcin (OCN) as bone formation markers (A). RANKL, osteoprotegerin (OPG) and carbonic anhydrase as degradation markers (B). β2-microglobulin (B2M) was used as a reference gene. The asterisks indicate (*) $p < 0.05$, (**) $p < 0.01$ and (***) $p < 0.001$ respectively.

was clearly demonstrated. This finding allows to conclude that the released Sr of the SrCPC cement is most likely to be responsible for higher new bone formation compared to the CPC group. This can be regarded as proof of principle that the local delivery of strontium from Sr-modified/loaded implants or biomaterials is possible and that strontium's biological activity to stimulate new bone formation is preserved within the CPC.

Ni et al. reported about the detection of Sr, Ca and further elements of a Sr-doped hydroxyapatite cement that was implanted into the proximal femoral intramedullary canal for 6 months by EDX and TOF-SIMS. However, there was only a maximum count rate for Sr of 3 in the 70 μm thick hydroxyapatite interface layer. In contrast to this study, we found a high release of Sr up to a distance of 5 mm to the implant. Sr, Ca and the collagen signal were found in the same areas of the newly formed bone suggesting that the released Sr from SrCPC was incorporated into the new bone.

The strontium modified calcium phosphate bone cement used in the present study has been developed recently by complete substitution of the $CaCO_3$ portion in the precursor mixture of a well-established, α-TCP based cement by $SrCO_3$. This simple approach which has been described in detail recently leads to a cement which releases strontium ions in relevant dosages *in vitro* [13]. A comparison of the *in vitro* strontium release and between the findings of the current animal trial is difficult. However, this *in vivo* study can demonstrate that a considerable amount of strontium is released from the SrCPC into the interface region and into the surrounding tissue which is most likely related to enhanced bone formation confirming the *in vitro* findings that biologically active doses of strontium can be released from SrCPC.

Regarding the *in vivo* degradation behavior of the materials, more and better fragmentation of the SrCPC compared to the CPC was found. This was associated with a statistically significant higher number of multinuclear cells in the SrCPC. With the assumption that at least some multinuclear cells are osteoclasts, it can be suggested that the SrCPC degradation process is not impaired by a potential anti-osteoclastic effect of the released Sr shown by reduction of RANKL expression in immunohistochemistry.

Biomaterials should be investigated in a clinically relevant model targeting their intended clinical use. Although most calcium phosphate cements are applied in fracture defects in patients, *in vivo* testing of these materials is mainly done in simple drill hole defects that does not represent clinically reality. The strength of the used animal model [14] is that it allows investigation of biomaterials in a clinically relevant situation. It exposes the materials to a fracture defect in the metaphyseal region of long bone rats. Internal fixation with the T-shaped plate on the distal femur also corresponds to the human situation. Ovariectomy and special diet was shown to lead to a significant reduction of bone mineral density compared to sham animals [14,17,18]. The materials are challenged with typical defect fracture healing processes for bone consolidation in this model under systemically impaired bone conditions. Compared to the previous study [14], we used a 4 mm fracture defect which could be shown to fulfill all requirements for a critical size defect in the empty defect control group as it did not show any bony consolidation after 6 weeks in this study. Therefore, the 4 mm fracture defect is a good model to study potential bone enhancement effects of biomaterials. Plate breakages in this model could be regarded as a drawback. However, even this fact links the model to clinical reality as plate breakages in the human situation are a typical sign for implant failure in case of impaired bone healing such as delayed or non-unions. Although, there was a non-statistically significant difference in plate breakages, with a p-value of $p = 0.06$ that there was a strong trend with fewer implant failure in the SrCPC compared to the CPC suggesting better bone healing for this parameter.

5. Conclusion

Both CPC and SrCPC revealed a statistically significantly enhanced new bone formation compared to the empty defect in a critical size defect in the metaphyseal area of the distal femur in ovariectomized rats. It could be shown that the SrCPC treated animals exhibited a statistically significant higher new bone formation both at the biomaterial–bone interface and in the entire fracture defect area compared to CPC. TOF-SIMS analysis could detect high count rates Sr from the SrCPC in the interface region and up to a distance of 6 mm to the implant which was not the case for CPC. This suggests that the enhanced new bone formation is attributable to local release from the SrCPC.

Acknowledgment

This study was supported by the Deutsche Forschungsgemeinschaft (DFG) SFB-TRR 79.

Appendix A. Supplementary data

Supplementary data related to this article can be found at http://dx.doi.org/10.1016/j.biomaterials.2013.07.036.

References

[1] Goldhahn J, Scheele WH, Mitlak BH, Abadie E, Aspenberg P, Augat P, et al. Clinical evaluation of medicinal products for acceleration of fracture healing in patients with osteoporosis. Bone 2008;43:343–7.

[2] Low KL, Tan SH, Zein SHS, Roether JA, Mouriño V, Boccaccini AR. Calcium phosphate-based composites as injectable bone substitute materials. J Biomed Mater Res B Appl Biomater 2010;94:273–86.

[3] Bonnelye E, Chabadel A, Saltel F, Jurdic P. Dual effect of strontium ranelate: stimulation of osteoblast differentiation and inhibition of osteoclast formation and resorption in vitro. Bone 2008;42:129–38.

[4] Marie PJ. Strontium ranelate: new insights into its dual mode of action. Bone 2007;40:S5–8.

[5] Andersen OZ, Offermanns V, Sillassen M, Almtoft KP, Andersen IH, Sørensen S, et al. Accelerated bone ingrowth by local delivery of strontium from surface functionalized titanium implants. Biomaterials 2013;34:5883–90.

[6] Xin Y, Jiang J, Huo K, Hu T, Chu PK. Bioactive srtio(3) nanotube arrays: strontium delivery platform on ti-based osteoporotic bone implants. ACS Nano 2009;3:3228–34.

[7] Zhao L, Wang H, Huo K, Zhang X, Wang W, Zhang Y, et al. The osteogenic activity of strontium loaded titania nanotube arrays on titanium substrates. Biomaterials 2013;34:19–29.

[8] Park J-W, Kim H-K, Kim Y-J, Jang J-H, Song H, Hanawa T. Osteoblast response and osseointegration of a ti-6al-4v alloy implant incorporating strontium. Acta Biomater 2010;6:2843–51.

[9] Park J-W, Kim Y-J, Jang J-H. Enhanced osteoblast response to hydrophilic strontium and/or phosphate ions-incorporated titanium oxide surfaces. Clin Oral Implant Res 2010;21:398–408.

[10] Park J-W, Kim Y-J, Jang J-H, Song H. Positive modulation of osteogenesis- and osteoclastogenesis-related gene expression with strontium-containing microstructured ti implants in rabbit cancellous bone. J Biomed Mater Res A 2013;101:298–306.

[11] Li Y, Li Q, Zhu S, Luo E, Li J, Feng G, et al. The effect of strontium-substituted hydroxyapatite coating on implant fixation in ovariectomized rats. Biomaterials 2010;31:9006–14.

[12] Fu D-L, Jiang Q-H, He F-M, Yang G-L, Liu L. Fluorescence microscopic analysis of bone osseointegration of strontium-substituted hydroxyapatite implants. J Zhejiang Univ Sci B 2012;13:364–71.

[13] Schumacher M, Henß A, Rohnke M, Gelinsky M. A novel and easy-to-prepare strontium(II) modified calcium phosphate bone cement with enhanced mechanical properties. Acta Biomater 2013;9:7536–44.

[14] Alt V, Thormann U, Ray S, Zahner D, Dürselen L, Lips K, et al. A new metaphyseal bone defect model in osteoporotic rats to study biomaterials for the enhancement of bone healing in osteoporotic fractures. Acta Biomater 2013;9:7035–42.

[15] Fletcher JS, Vickerman JC. Secondary ion mass spectrometry: characterizing complex samples in two and three dimensions. Anal Chem 2013;85:610–39.

[16] Vickerman JC, Briggs D. ToF-SIMS: surface analysis by mass spectrometry. Chichester: IM; 2001.

[17] Heiss C, Govindarajan P, Schlewitz G, Hemdan NYA, Schliefke N, Alt V, et al. Induction of osteoporosis with its influence on osteoporotic determinants and their interrelationships in rats by DEXA. Med Sci Monit 2012;18:BR199–207.

[18] Schlewitz G, Govindarajan P, Schliefke N, Alt V, Böcker W, Elkhassawna T, et al. Ovariectomy and calcium/vitamin D2/D3 deficient diet as a model of osteoporosis in the spine of sprague-dawley rats. Z Orthop Unfall 2013;151:14–9.

[19] Driessens FCM, De Maeyer E, Fernandez E, Boltong M, Berger G, Verbeeck R, et al. Amorphous calcium phosphate cements and their transformation into calcium deficient hydroxyapatite. Bioceramics 1996;9:231–4.

[20] Sanni OD, Wagner MS, Briggs D, Castner DG, Vickerman JC. Classification of adsorbed protein static tof-sims spectra by principal component analysis and neural networks. Surf Interface Anal 2002;33:715–28.

[21] Peters A, Toben D, Lienau J, Schell H, Bail HJ, Matziolis G, et al. Locally applied osteogenic predifferentiated progenitor cells are more effective than undifferentiated mesenchymal stem cells in the treatment of delayed bone healing. Tissue Eng Part A 2009;15:2947–54.

[22] Pfaffl MW, Horgan GW, Dempfle L. Relative expression software tool (REST©) for group-wise comparison and statistical analysis of relative expression results in real-time PCR. Nucleic Acids Res 2002;30:e36.

[23] Vestermark MT, Hauge E-M, Soballe K, Bechtold JE, Jakobsen T, Baas J. Strontium doping of bone graft extender. Acta Orthop 2011;82:614–21.